350284 8P N95-14569

THE EXTENSIONAL RHEOLOGY OF NON-NEWTONIAN MATERIALS

Stephen H. Spiegelberg, Samuel Gaudet, and Gareth H. McKinley

Division of Applied Sciences
Harvard University
Cambridge, MA 02138

ABSTRACT

It has been proposed to measure the extensional viscosity function of a non-Newtonian polymer solution in a reduced gravity environment as part of the Advanced Fluid Module. In ground-based extensional measurements, the no-slip boundary condition at solid-fluid interfaces always results in appreciable shear gradients in the test fluid; however the removal of gravitational body forces permits controlled extensional deformation of containerless test samples and the first unambiguous measurements of this kind. Imperative to successful implementation of this experiment is the generation and subsequent deformation of a stable cylindrical column of test fluid. A study of the generation and deformation of liquid bridges demonstrates that Newtonian liquid bridges undergo capillary breakup as anticipated when stretched beyond a critical aspect ratio; non-Newtonian liquid bridges, however, are stabilized by the strain-hardening phenomenon exhibited by these materials. Numerical simulations of Newtonian breakup are compared with experimental results, and show that previous ground-based attempts at measuring the extensional viscosity of Newtonian fluids are of limited accuracy.

INTRODUCTION

The prevalence of extensional flows in common polymer-processing operations such as extrusion, blow-molding and fiber-spinning has motivated the investigation of the rheological properties of non-Newtonian fluids under idealized extensional flow conditions. Unlike Newtonian fluids, these materials cannot be characterized by a single material parameter such as the Newtonian viscosity μ, and the non-linear response must be characterized over a wide range of carefully-controlled deformations. A rigorous continuum mechanical consideration of the displacement gradients in a viscoelastic material shows that all possible deformations can be represented in terms of the invariants I_1 and I_2 of the finite finger strain tensor [1]. In this parameter space it is found that the strain invariants for homogeneous shear-free deformations do not intersect with those of simple-shear deformations for any non-zero deformation rates. The rheological functions that relate shear-free deformations to stresses in the fluid are therefore fundamental material properties of a non-Newtonian fluid and need to be measured independently from the viscometric shear-flow functions $\eta(\dot{\gamma})$, $\Psi_1(\dot{\gamma})$, and $\Psi_2(\dot{\gamma})$, which represent the shear viscosity, and the first and second normal stress components of the fluid.

The uniaxial extensional stress growth material function $\overline{\eta}^+$, or the *transient extensional viscosity*, is defined as

$$\tau_{zz}(t)-\tau_{rr}(t)=\overline{\eta}^+(t,\dot{\varepsilon}_0)\dot{\varepsilon}_0 \tag{1}$$

where $\tau_{zz}(t)-\tau_{rr}(t)$ is the time-varying normal or tensile stress difference, and $\dot{\varepsilon}_0$ is the constant imposed extensional strain rate. In the limit $t \to \infty$, the transient extensional viscosity approaches the steady state value $\overline{\eta}(\dot{\varepsilon})$. To achieve a homogeneous shear-free flow, all off-axis velocity gradient must be zero and the fluid elements must be elongated along the z–axis such that the rate of strain is independent of position. The velocity field for such a deformation may be represented in a general form as [1];

$$v_r=-\tfrac{1}{2}\dot{\varepsilon}_0 r \qquad v_\theta=0 \qquad v_z=\dot{\varepsilon}_0 z \tag{2}$$

and the Lagrangian separation $L(t)$ of two neighboring fluid points initially separated by a distance L_0 is given by

$$L(t)=L_0 e^{\dot{\varepsilon}_0 t} \tag{3}$$

Numerous experimental configurations have been devised to realize such kinematics and measure the resulting dynamic properties that characterize the extensional material functions of complex fluids (see Gupta and Sridhar [2]

and Meissner [3] for details). All the configurations considered to date have a fundamental physical constraint – the need for a solid container that holds the test fluid in a given position or geometric shape under the action of an external gravitational body force. The frictional boundary conditions that applies along all contact points of a liquid-solid interface results in large shearing forces that mask any extensional response of the fluid. This constraint will be almost entirely absent in a microgravity environment.

Removal of gravitational body forces will greatly simplify the measurement of the response of a complex fluid to a uniaxial extensional deformation. The experiment reduces to three fundamental steps: *(i)* generation of a column of test liquid; *(ii)* imposition of the deformation kinematics specified in equation (2); and *(iii)* measurement of the tensile stress difference in the elongating fluid column. The transient extensional viscosity may then be computed from equation (1).

In this paper we present results from the first phase of this project, namely the generation and controlled deformation of a fluid column in the absence of container boundaries. We present an experimental ground-based study of liquid bridge stability, and compare the results to numerical simulation. The results show that strain-hardening significantly stabilizes non-Newtonian liquid bridges against capillary breakup.

EXPERIMENTAL

Test fluid

Two viscous test fluids have been examined in this study. The first is a non-Newtonian test fluid composed of 0.31% polyisobutylene (Mw ≈ 1.7 x10^6 g/mole, polydispersity index ≈ 1.9) dissolved in low molecular weight Newtonian solvent of hydrogenated polybutene. This semi-dilute polymer solution falls into a class of fluids termed *Boger fluids*, which exhibit a nearly constant shear viscosity over several decades of shear rate, yet are highly elastic [4]. The second fluid used in the study consists simply of the Newtonian solvent (polybutene) as a reference standard. The density of both fluids is ρ = 0.894 g/ml as determined *via* hydrometry. The zero shear viscometric data for the two fluids, as determined from cone & plate rheometry with a Rheometrics Mechanical Spectrometer RMS-800 are shown in Table 1 at a reference temperature of 25°C.

Apparatus

Figure 1 shows a schematic diagram of the device used to generate the liquid bridges. The test fluid is charged into the cavity (1) created when the acrylic sleeve is restored to the closed position (*i.e.* slid to the right in Figure 1). The liquid bridge is formed *via* positive displacement as the sleeve is slowly withdrawn to the left. In the current configuration, liquid bridges with a diameter of $D_0 = 2R_0$ = 3.80 cm may be generated. The moveable piston (2) allows the formation of bridges of varying length (corresponding to dimensionless aspect ratios from $L/D \equiv \Lambda$ = 0 to 3.3), as well as the elongation of a previously-generated bridge. The piston drive shaft is connected to a DC servomotor driven by a computer controlled motion controller. Figures 2*a* and *b* show typical examples of a liquid bridge before and after an elongational deformation.

All of the ground-based experiments have been carried out in a *Plateau Tank* [5] consisting of a constant temperature bath filled with an immiscible fluid that is carefully density-matched to the test fluid, in effect creating a microgravity environment. For this experiment, the neutral density fluid (NDF) was composed of approximately 60% 1-propanol (ρ = 0.806 g/ml) and 40% water. The maximum *Bond Number* for this system, defined as the ratio of buoyancy forces to surface tension forces, was approximately $Bo = \Delta\rho g R_0^2/\sigma \approx 0.1$.

In addition to the Bond number, the dynamic properties governing the extensional deformation of the liquid bridge may be characterized by several dimensionless groups, namely the *Capillary number* (ratio of viscous stresses/interfacial stresses), the *Reynolds Number* (ratio of inertial stresses/viscous stresses), and the *Deborah Number* (time scale of fluid/time scale of deformation). These terms are defined as:

$$Bo = \Delta\rho g R_0^2/\sigma \qquad Re = \rho R_0 U_P/\eta_0$$
$$Ca = \eta_0 U_P/\sigma \qquad De = \lambda_1 \dot{\varepsilon}_0 \tag{3}$$

where R_0 is the column radius, U_P is the characteristic velocity imposed by the piston; ρ, σ and η are the test fluid density, surface tension and viscosity respectively, λ_1 is a characteristic relaxation time of the non-Newtonian fluid, and the characteristic stretch rate experienced by the fluid is $\dot{\varepsilon}_0$.

To date, only a linear stretch history has been imposed in the experimental section of this work; *i.e.* the sample length $L(t)$ increases linearly with time; the characteristic stretch rate $\dot{\varepsilon}_0 \sim U_P/L(t)$ thus decreases during the deformation. In the numerical simulations, however, both a linear and an exponential stretch history have been examined. In the latter case, the piston velocity is ($U_P = \dot{\varepsilon}_0 Z_P$) and the length increases in time as $L = L_0 \exp(+\dot{\varepsilon} t)$ This deformation history produces a constant extension rate everywhere in the sample, if the sample remains cylindrical.

Calculations

In a previous paper we have described the implementation of the boundary integral method to investigate the dynamic evolution of deforming liquid filaments and the breakup of viscous (low Reynolds number) Newtonian fluid columns stretched beyond a critical aspect ratio [6]. The fluid motion is characterized by the capillary number, the initial and final aspect ratios (Λ_0, Λ_f) of the column, and the viscosity ratio of the fluid column (μ_2) compared to the outer fluid bath (μ_1).

RESULTS AND DISCUSSION

Newtonian and non-Newtonian liquid bridges have been subjected to identical deformation histories to assess the effects of extensional hardening on bridge stability. Liquid bridges with an initial aspect ratio of $\Lambda_0 = 0.87$ and a dimensionless volume $\mathcal{V} \equiv V_0/\pi R_0^2 L = 1$ were stretched to a final aspect ratio of 2.00 at a constant velocity of $U_P = 0.13$ mm/s corresponding to a capillary number of $Ca = 0.19$. Since the deformation rate varies throughout the test, the Deborah number decreases from 0.011- 0.006.

Figure 3 shows photographs of the evolution of the liquid bridge interfaces as of a function of time for the two test fluids. The photographs labeled as '0 minutes' correspond to the bridge immediately after cessation of the steady stretch; during the ensuing pictures, the bridges experiences no additional stretching but continue to evolve towards their final static equilibrium configuration. During the initial deformation, the fluid column adopts a concave cylindrical configuration, due to the fixed volume of fluid and the pinning condition experienced at the endplates. After 15 minutes, both bridges have relaxed to a surface energy–minimizing unduloid configuration. The non-Newtonian fluid retained this shape for the remainder of the experiment, up to times of 20 hours. Longer periods of μg are difficult to maintain due to evaporation and thermal gradients in the Plateau tank. The Newtonian fluid, however, experienced continual constriction in the center of the bridge; this constriction accelerates over the course of the experiment, and eventually results in bridge break-up after 173 minutes.

This hydrodynamic instability was first discussed for inviscid fluids by Lord Rayleigh [7], who predicted using surface energy arguments that cylindrical fluid filaments with $\Lambda > \pi$ were susceptible to random sinusoidal perturbations that acted to reduce the surface area of the cylinder; runaway capillary breakup ensued. Gillette and Dyson [8] extended this analysis to non-cylindrical bridges constrained between equal circular plates, and presented a stability envelope for constricted bridges, in terms of dimensionless sample volume $\mathcal{V}$ *vs.* aspect ratio Λ. The bridges shown in Figure 3 correspond to loci initially in the stable region of this stability diagram, which were subsequently stretched along a hyperbolic path $\mathcal{V}\Lambda$ = *constant* into the unstable region.

In the constricted region of the bridge, capillary pressure increases as the radius of curvature decreases. This increased pressure drives fluid out of the neck region into the lower pressure areas near the endplates, and therefore reduces the radius in the constricted region even more. The process accelerates as the radius of curvature decreases, eventually resulting in sample failure. It is clear that the stability of the non-Newtonian fluid bridge is not governed by identical arguments, since the bridge remained intact despite the fact that purely from energetic considerations of fluid statics it was also deformed beyond the Gillette & Dyson stability locus. The non-Newtonian strain hardening nature of the Boger fluid leads to this restabilization of the liquid bridge; the transfer of fluid from the constricted region of high pressure to lower pressure regions results in a uniaxial extensional flow. Under such conditions a Newtonian fluid has a steady extensional viscosity of $\bar{\eta} = 3\mu$ [9]; however, measurements for non-Newtonian fluids indicate that the viscosity will rise by 3 or more orders of magnitude [10]. This rise in viscosity effectively retards the flow of fluid, and thus stabilizes the liquid bridge from any further constriction.

Numerical calculations described elsewhere [6] were utilized to simulate the experimentally-observed breakup of the Newtonian liquid bridge following imposition of an identical deformation to that described above. The narrowest radius of the bridge in the middle of the constricted region (R_{mid}) is shown in Figure 4 as a function of dimensionless time. The initial rapid decrease in radius occurs during the imposed extensional deformation of the

bridge up to a dimensionless time given by $\sigma t/\mu R_0 \sim 1$. Capillary forces progressively reduce the radius in the remainder of the experiment. It can be seen that the results from the simulation correlate remarkably well with the experimental results; deviations are seen only at the end of the experiment when the length scale of the filament becomes small. Under such conditions, the experimental error increases and the numerical method also becomes increasingly inaccurate.

Having validated the accuracy of the boundary element method, additional numerical calculations have been performed to investigate the behavior of a Newtonian liquid bridge under an *exponential* imposed deformation. Such tests have been proposed as a method for measuring the extensional viscosity of viscous fluids [10, 11]. Measurement of the net traction force on the endplate (after a correction for the contribution of surface tension forces) yields an estimate of the extensional viscosity of the fluid. In Figure 5(a) we show the axial free-surface profile *R(z)* and axisymmetric velocity field in an elongating liquid bridge with initial aspect ratio $\Lambda_0 = 0.6$ after a dimensionless strain of 2. It is clear from these calculations that the velocity field is not an homogeneous uniaxial elongation because of the three-phase contact line that pins the fluid interface to the edge of the piston. At large strains this deformation becomes increasingly important and in Fig. 5(b) we show an expanded view of the weak flow near the stationary left-hand piston indicating that a *flow reversal* can develop. This recirculation reverses the sign of the viscous contribution to the traction force exerted on the end plate, and results in substantial deviation of the calculated transient Trouton ratio $T_R = \overline{\eta}^+(\dot{\varepsilon}_0, t)/\mu$ from the predicted value of $T_R \equiv 3$ for a Newtonian fluid. Similar calculations for non-Newtonian liquid bridges are currently underway.

CONCLUSIONS

We have presented measurements and simulations of the stability of both Newtonian and non-Newtonian fluids in a reduced gravity environment. Newtonian bridges experience immediate breakup when stretched beyond a critical aspect ratio and undergo capillary breakup in good agreement with the predictions of classical energetic stability arguments and boundary element calculations. Non-Newtonian fluid bridges with similar shear viscosities exposed to identical stretching histories did not breakup, but rather were stabilized by the strain-hardening extensional viscosity exhibited by these materials. It is clear that selection of an initial aspect ratio will be critical when performing extensional flow measurements in the Newtonian case to ensure an initially stable column. This research represents a preliminary ground-based investigation forming part of the Science Requirement Document (SRD) submitted to NASA for a proposed microgravity flight experiment to measure the extensional viscosity of non-Newtonian polymer solutions.

ACKNOWLEDGEMENTS

This research was supported by the Microgravity Fluid Physics branch of MSAD at NASA–LeRC. The authors would like to thank Prof. Howard. A. Stone for his invaluable help with implementation of the boundary element formulation discussed herein.

REFERENCES

(1) Petrie, C. J. S. *Elongational Flows: Aspects of the Behavior of Model Viscoelastic Fluids*; Pitman: London, 1979; Vol. 29.
(2) Gupta, R. K.; Sridhar, T. In *Rheological Measurement*; ed.; A. A. Collyer and D. W. Clegg, Ed.; Elsevier Applied Science: London, 1988; pp 211-245.
(3) Meissner, J. *Chem. Eng. Commun.*, **33**, 159-180, (1985).
(4) Boger, D. V. *J. Non-Newtonian Fluid Mech.*, **3**, 87-91, (1977/78).
(5) Plateau, J. A. F. In *Ann Rep. Smithsonian Institution*1863; pp 207-285.
(6) Gaudet, S.; McKinley, G. H.; Stone, H. A. In *AIAA, 32nd Aerospace Sciences*; Reno, NV, 1994; p 1.
(7) Rayleigh, L. *Proc. Lond. Math. Soc.*, **10**, 4-13, (1879).
(8) Gillette, R. D.; Dyson, D. C. *Chem. Eng. J.*, **2**, 44-54, (1971).
(9) Trouton, F. T. *Proc. Roy. Soc.*, A77, 426, (1906).
(10) Tirtaatmadja, V.; Sridhar, T. *J. Rheol.*, **37**, 1081, (1993).
(11) Sridhar, T., Tirtaatmadja, V., Nguyen, D.A. and Gupta, R.K., *J. Non-Newtonian Fluid Mech.*, **40**, (1991), 271-280.

Table 1: Physical properties of 0.31 wt.% PIB/PB Boger fluid at T_0 = 25°C.

Viscometric Properties	η_0 [Pa.s]	47.2
	η_s [Pa.s]	43.2
	Ψ_{10} [Pa.s^2]	20.3
	Ψ_2 [Pa.s^2]	0
Bulk Properties	ρ [kg/m^3]	894
	σ [N/m]	3.0×10^{-3}
Oldroyd-B Model Parameters	λ_1 [s]	2.54
	β	0.92

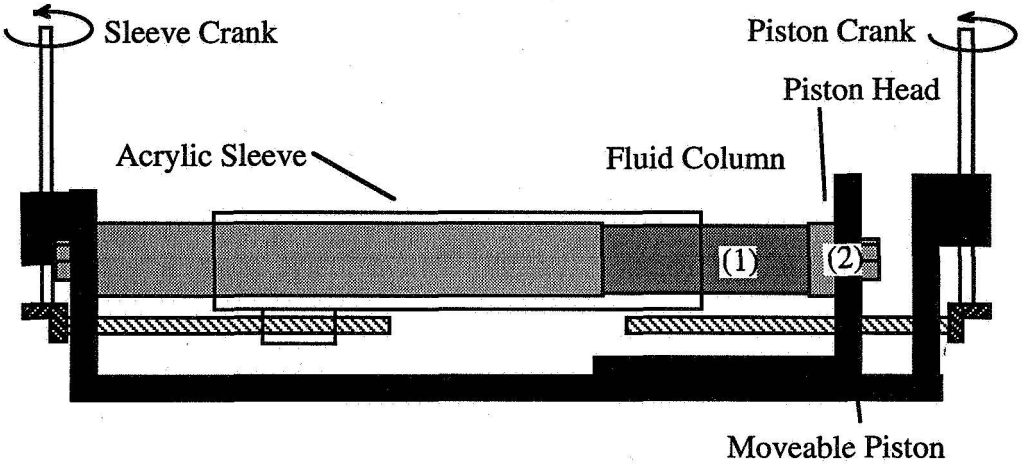

Figure 1: Device for generation of liquid bridges. Fluid is charged into cavity created by acrylic sleeve, which is then withdrawn to expose sleeve to air or fluid interface. Bridge can be stretched with translating piston.

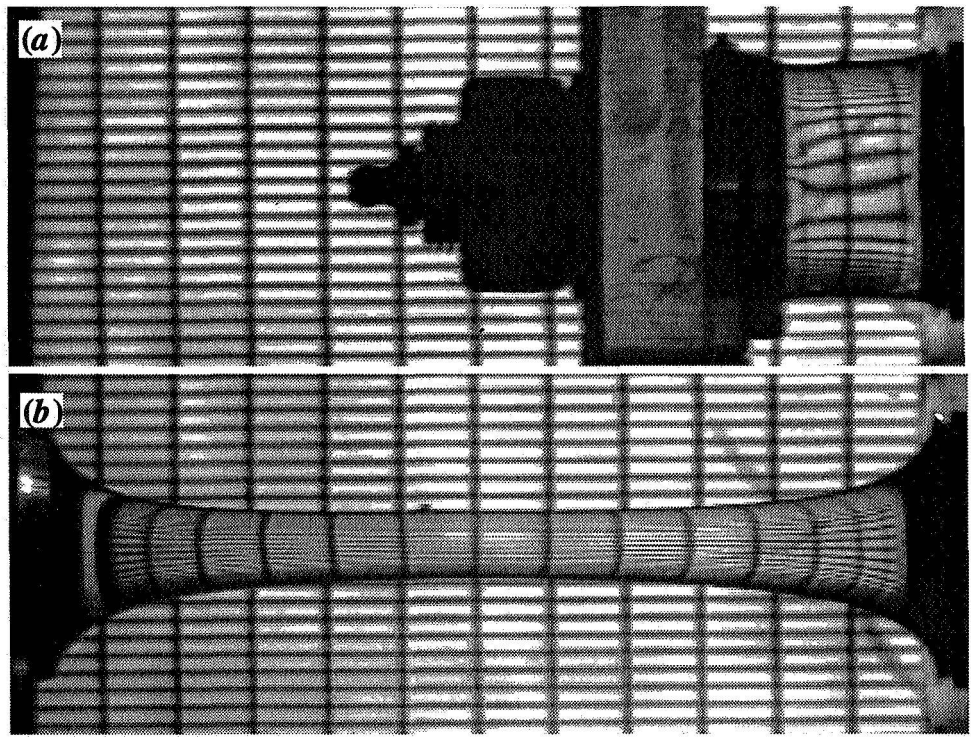

Figure 2: Non-Newtonian liquid bridge from Λ_0 = 0.46 to Λ_f = 3.10 at a constant strain rate of 0.02 s^{-1} corresponding to a De = 0.05, Ca_{max} = 2.9, and Bo = 0.1.

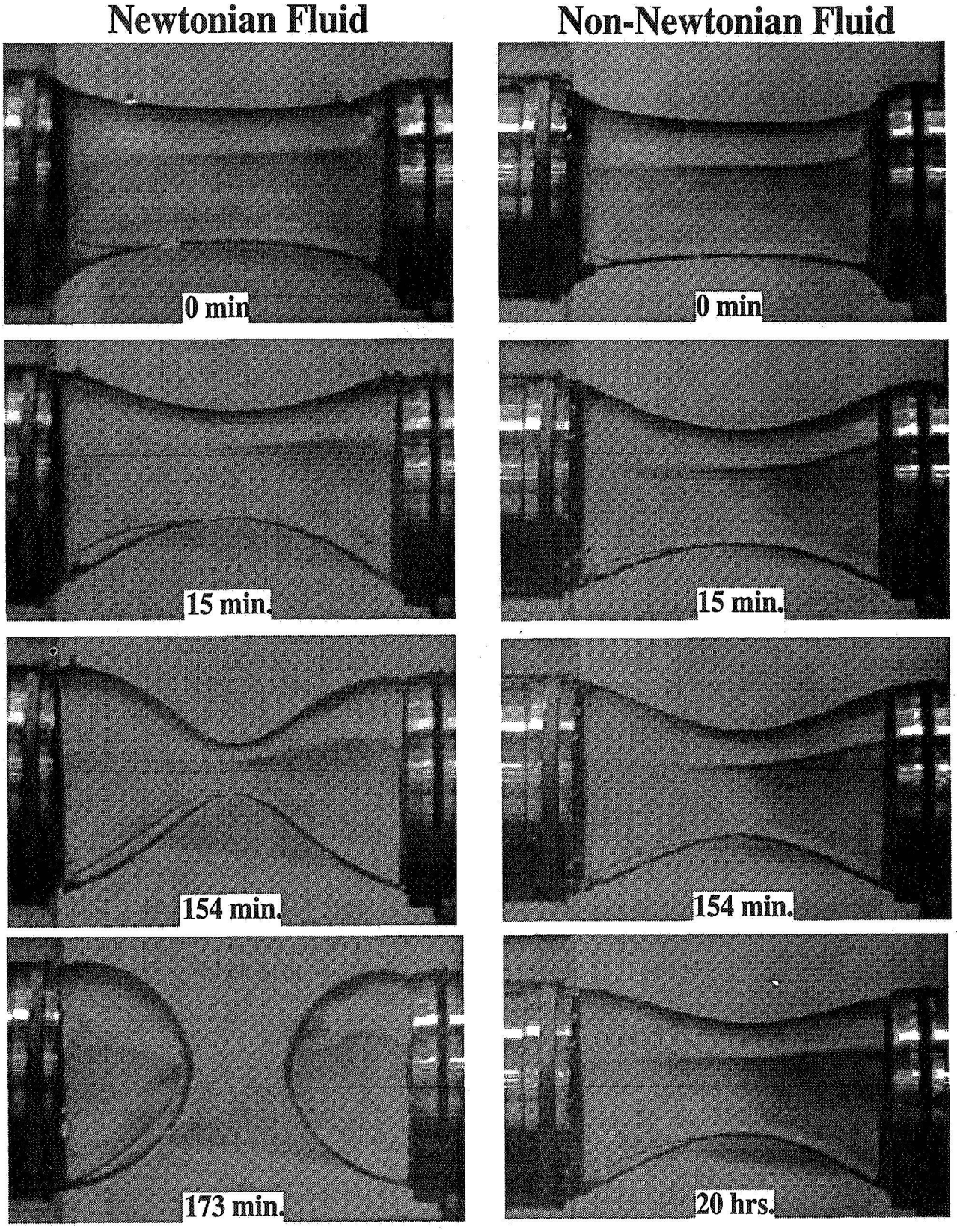

Figure 3: Liquid bridge stability evolution for Newtonian and non-Newtonian fluids. A_0 = 0.87, A_f = 2.00, Bo = 0.1.

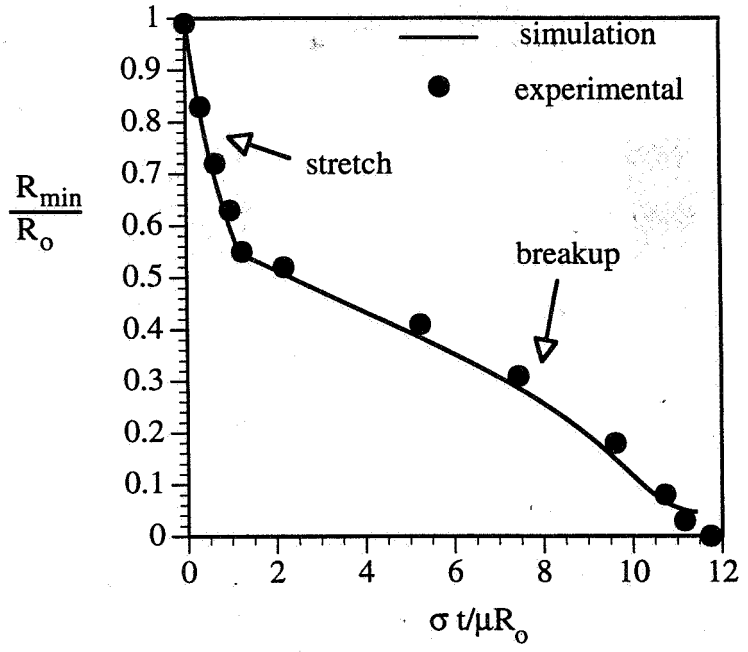

Figure 4: Neck radius of Newtonian liquid bridge as a function of dimensionless time. Radius decreases initially due to bridge stretch, then is further reduced by capillary forces. Bridge was stretched from an initial radius R_0 of 1.9 cm at a rate of 0.013 cm/s, corresponding to a Ca = 0.19. Bo = 0.1.

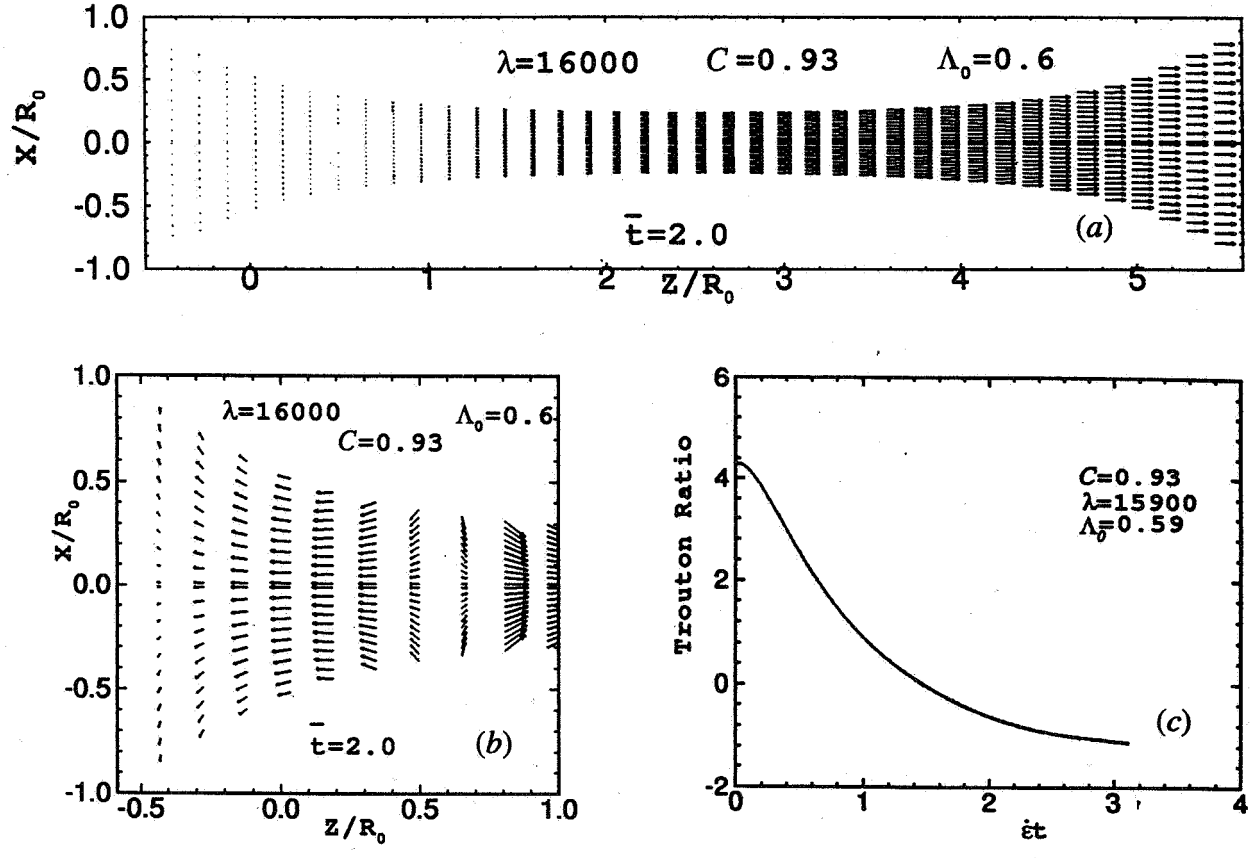

Figure 5: Extensional deformation of a Newtonian liquid bridge; (*a*) Final aspect ratio after a strain of $\dot{\varepsilon}_0 t$=2.0; (*b*) magnification of flow reversal near stationary end plate ; (*c*) calculated Trouton ratio $\bar{\eta}(\dot{\varepsilon}_0,t)/\mu$.